Available online at www.sciencedirect.com
SCIENCE DIRECT®
Journal of the European Ceramic Society 25 (2005) 163–174
www.elsevier.com/locate/jeurceramsoc

Modelling polymer-derived ceramics

Peter Kroll*

Institut für Anorganische Chemie, Rheinisch-Westfälische Technische Hochschule Aachen (RWTH), Professor-Pirlet-Strasse 1, 52056 Aachen, Germany

Available online 11 September 2004

Abstract

We investigate structure, energy, and elastic properties of some polymer-derived nitride ceramics, amorphous silicon nitride, a-Si_3N_4, and its ternary derivatives a-$Si_3B_3N_7$, a-SiNO, and a-SiCN. Model structures consist of 104–448 atoms. They are first generated by an empirical network algorithm and then further computed using density functional methods including extensive ab initio molecular dynamics simulations. Optimized structures we obtain exhibit perfect chemical order consistent with the perception of an inorganic network derived from polymer precursors. We find a random network structure for a-SiNO, but phase segregation of BN and C sub-structures in a-$Si_3B_3N_7$ and a-SiCN, respectively. The phase partitioning is driven by energy and benefits from a low density of the material, since we find the segregated phase predominantly at internal surfaces of voids and pores. Energies calculated for a-SiCN phases support a non-solubility of carbon in a-Si_3N_4 or stoichiometric a-SiCN. The bulk modulus of a-$Si_3B_3N_7$ and a-SiCN is comparable to that of a-Si_3N_4 but at 5–10% lower density of the material.

Keywords: Polymer-derived ceramics; Silicon; Ternary derivatives

1. Introduction

In recent years, polymer thermolysis became of increasing interest for the synthesis of new inorganic materials.[1,2] Non-oxide ceramics are one focus of investigations because of their covalent bonding providing mechanical reliability and high-temperature stability. There are numerous milestones set by the community already out of which we refer to two landmarks that indicate the perspectives of polymer-derived ceramics.[3,4] Further references to the literature will be given by authors of excellent papers in this special issue of the Journal of the European Ceramic Society.

The amorphous state of these materials is of great importance for their properties. Synthesized from polymers, all nitride ceramics remain amorphous at least up to 1000 °C. Even at higher temperatures, when phase partitioning starts and precipitation of crystalline phases occurs, the vast majority of the material is featureless and amorphous. Some materials retain a predominantly amorphous structure up to 2000 °C.[3,4] The structure of these amorphous materials at the atomic level, however, is still veiled to great extend. Increasing efforts are made to characterize the structure to achieve a better understanding and to find ways to further improve the materials properties. The signals obtained in the experiment, broad probability distributions which carry all the information about the manyfold of chemistry and physics of the amorphous structure, can rarely be transformed back into individual contributions. We seek, however, the details of the atomistic structure to understand the materials properties at the fundamental level. The disordered state, therefore, provides fertile soil for structural modelling and computational studies, not at least to further a meaningful interpretation of experimental data.

Our perception of the atomistic structure of amorphous materials is based on Zachariasen's model of vitreous silica introduced some 70 years ago (see Fig. 1).[5] We expect a network composed of atoms and bonds that fulfills basic requirements for the local environment in terms of coordination, bond distances, and bond angles. As to whether the network is of random nature or whether it exhibits some partitioning already in the disordered state – probably depending on the synthesis strategy – is a question necessary to be concerned of.

* Tel.: +49 241 8090066; fax: +49 241 8092288.
E-mail address: peter.kroll@ac.rwth-aachen.de.

0955-2219/$ – see front matter © 2004 Elsevier Ltd. All rights reserved.
doi:10.1016/j.jeurceramsoc.2004.07.012

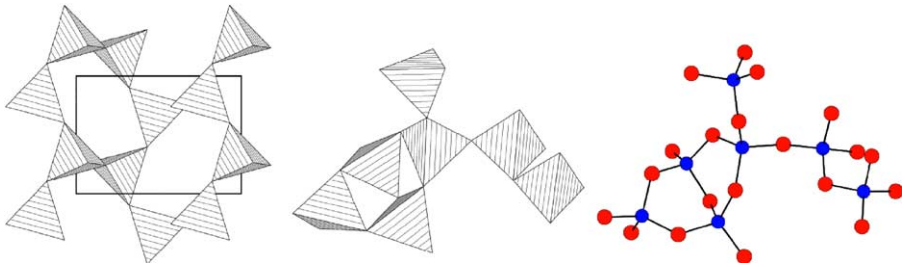

Fig. 1. The model structures to illustrate Zachariasen's model of silica glass and the concept of a chemically ordered network: The tetrahedral arrangement in the structure of quartz is shown on the left side. The same motif of tetrahedra is present throughout the structure of vitreous silica, however, connected in a disordered an irregular fashion. Resolved into a model consisting of atoms and bonds, the structure comprises a network perfectly ordered and alternating in Si and O.

Our approach to model the amorphous structure of polymer-derived ceramics then exploits the idea of a chemically ordered random network structure. We first generate a network, introducing a well-defined local order for every element, and then access structure, properties and structural evolution including a possible phase partitioning towards a network with non-random nature at elevated temperatures. Our concept, therefore, is opposite to the approach of generating an amorphous model by quenching a melt-like liquid, be it with empirical potentials,[6–8] semi-empirical methods,[9] or ab initio molecular dynamics simulations.[10] From several advantages, its speed and the capability of strictly defining a local bonding environment, e.g. no N–N bonds or setting the ratio sp^3-C:sp^2-C, allow us to test different hypotheses about the amorphous structure by doing multiple approaches. In this paper we will present on our most recent results for a-Si_3N_4, a-$Si_3B_3N_7$, a-SiNO, and a-SiCN. We will focus on structure and energy, and will furthermore access the bulk modulus as a representative measure for the elastic properties of the material.

2. Computational method

Our approach to model the amorphous structure of polymer-derived materials consists of two steps. First we generate *continuous random networks* with well-defined local coordination for all atoms. The network structures exhibit a perfect chemical order, but no symmetry elements except for the periodic boundaries of a large simulation box. Consequently, a-Si_3N_4 exhibits Si–N bonds only, a-$Si_3B_3N_7$ is built up from Si–N and B–N bonds, and there are only Si–N and Si–O bonds in our models of a-SiNO. The perfect chemical order in these three phase systems results in an alternating network, in which each cation is surrounded by anions only and vice versa, that exhibits even-membered rings only. In models of a-SiCN with composition $Si_{40}C_{40}N_{40}$, we include Si–N, Si–C, C–N, and C–C bonds. These network structures comprise both even- and odd-membered rings. The networks are constructed with a modified bond-switching algorithm.[11] We used both *topological* and *geometrical* relaxations, combined in a Monte Carlo/Molecular Dynamics (MC/MD) hybrid-method. The cost function we introduce is a simple Keating-type potential including additional repulsive interactions that allows for a rapid evaluation of energy and forces. Typically, we evaluate 10^7–10^8 bonding configurations in a simulated annealing approach to explore the phase space and to locate minimum energy configurations. The density of the network structures can, to some extend, be "directed" by fixing the box dimensions for almost the entire generation procedure, allowing cell optimization only during the final stage of modelling. Details of the implementation of the algorithm are given elsewhere.

In a second step, we use these network models as initial configurations for an optimization and annealing scheme within density functional theory[12] using pseudopotentials, plane waves, and the local density approximation (LDA)[13] as implemented in the Vienna Ab-initio Simulation Package.[14–17] First, the networks are relaxed in order to obtain optimized structural models. Then we perform ab initio molecular dynamics simulations (using the time-step Δt = 1 fs) at constant volume at elevated temperatures 800–2600 °C to evaluate structural and chemical stability of the models and to investigate the evolution of the structures. For any temperature in the ab initio molecular dynamics we ensure to have reached a "pseudo-converged" state. Thus, within the next 2–5 ps no further changes in energy or structure do happen. We increase the temperature usually only after having reached this requirement. Consequently, temperatures we refer to do not correspond to experimental temperatures of a typical tempering process, since the ensemble we calculate can never reach an equilibrium state within the time-scale available of ab initio molecular dynamics simulation (some 10–100 ps). We observe, nevertheless, "melting" (defined as rapid diffusion of the atoms) and very different chemical reactions depending on the temperature, that then may resemble the different activation energies for such processes. After every 1 or 2 ps in the ab initio molecular dynamics we investigate the underlying potential energy surface of our models by a rapid quench, allowing for complete optimization of positions and cell shape. For more details of the computational procedure we refer to one of our most recent publications.[18] Due to the size of the models (lattice constants are usually larger than 10 Å, the volume always larger

than 1000 Å^3) and the nature of first-row atoms carbon, nitrogen, and oxygen, the calculation of the amorphous models are highly demanding in terms of computing resources. For example, 1000 time steps (1 ps) ab initio molecular dynamics of a 112-atom model of a-Si_3N_4 require about 48 cpu-hours on a typical 1.5 GHz processor. The computation of the bulk modulus of one a-SiNO model with about 120 atoms is done through full optimizations at nine different volumes, each using about 24 cpu-hours and approximately 1 GB of memory. The 448-atom model of a-Si_3N_4 needs a memory of more than 2 GB during relaxation; 20 time steps ab initio molecular dynamics are done on the IBM-Regatta with 16 processors in parallel in about 3 h. All calculations were carried out on Super-Computers, the Aachen SunFire-Cluster and the Cray-T3E and IBM-Regatta-Cluster at the FZ Jülich.

3. Results

3.1. *a-Si_3N_4*

Of the models of a-Si_3N_4 consisting of 112 atoms each that we generated using our network approach and subsequently optimized, annealed extensively at elevated temperatures up to 2000 °C and re-optimized, two representatives are shown in Fig. 2. Both structures exhibit a perfect chemical order: only Si–N bonds, but no Si–Si or N–N bonds are present. The two structures have very different densities, 3.2 g/cm^3, which approaches the density of the crystalline phases of Si_3N_4 (we calculate ρ(β-Si_3N_4) = 3.16 g/cm^3) and 2.6 g/cm^3. The low density was achieved by increasing the volume of simulation cell already in the empirical generation scheme. Consequently, internal voids developed that interconnected to form a pore in our 112-atom models. Larger sized models (224 or 448 atoms) show a smaller tendency to form pores at the same density. Thus, the smaller the model, the more likely it is that voids will interconnect through the periodic boundaries to form a pore. Such porous models can be utilized to study catalytic reactions in porous silicon imidonitrides.[19]

Structural rearrangements did occur in all a-Si_3N_4 models during the optimization and annealing procedure. A consequence of this is the presence of some topological defects. Generally, the number of defects in our models are small, but the results we obtained from eight 112-atom models is further augmented by two models with 224 atoms and one model with 448 atoms. The dominating topological defect in all these structures is a four-fold coordinated N atom, $N^{[4]}$, that is found for about 7% of all N atoms. Approximately 4% of the N-atoms are two-fold coordinated, $N^{[2]}$. We also find about 4% five-fold coordinated Si atoms, $Si^{[5]}$. The three-fold coordinated Si atom, $Si^{[3]}$, is a very rare species in our models generated from network. We observe it only for about 1% of all Si atoms. Some models we received are free of $Si^{[3]}$. Summing up, this leads to an average connectivity for Si of 4.01 and for N of 3.01.

The definition of local connectivity is to some extend arbitrary. While the typical bond length Si–N is 173 pm, we observed several Si–N bonds at 210 pm. The bonding character of this configuration was indicated by a pyramidal Si environment with the apex pointing to a fourth nitrogen atom. Analysis of the charge distribution, furthermore, reveals a bond. The interaction of both sites is supported by the dynamic evolution observed in ab initio molecular dynamics at room temperature. A true three-coordinated silicon atom in a-Si_3N_4 thus remains a rare object. With a defect concentration of 1% of all Si atoms, however, we are still at the upper boundary of the experimental result. Electron Spin Resonance (ESR) data supports a defect concentration of 10^{17} to 10^{20} cm^{-3}.[20]

If we compare the initial structure as provided by the empirical network algorithm with the geometry finally optimized, this resulted in a significant gain in bonding

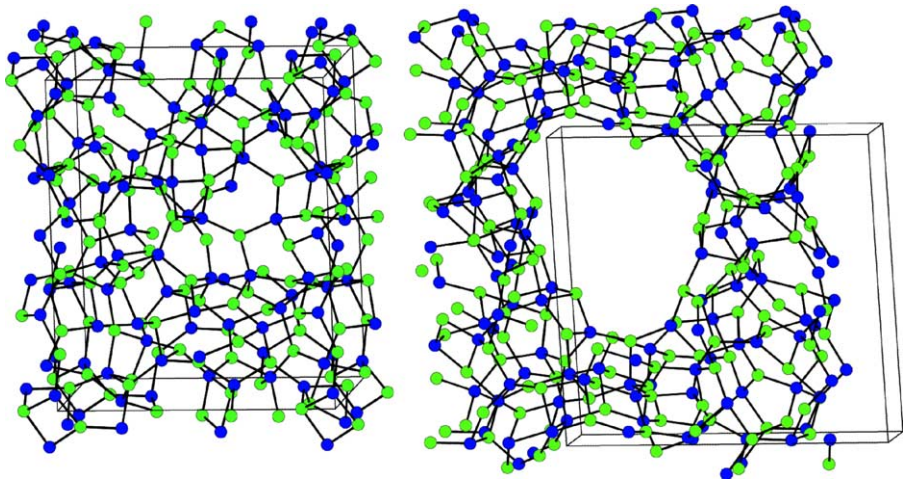

Fig. 2. Two models of a-Si_3N_4 with 112 atoms each in the simulation cell. The model on the left side has the density ρ = 3.2 g/cm^3, the one one the right has ρ = 2.6 g/cm^3. Dimensions of the simulation cell are 11.7 Å × 10.2 Å × 9.6 Å, and 8.7 Å × 13.2 Å × 12.5 Å, respectively. The boxes are close to rectangular, 85° < α, β, γ < 94°. Blue circles are Si, green circles are N atoms.

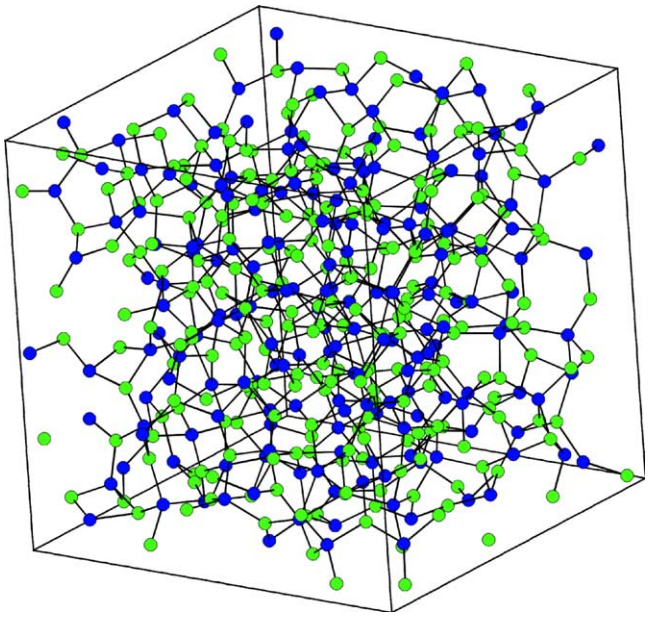

Fig. 3. Model of a-Si_3N_4 with 448 atoms in the simulation cell. Its density is ρ = 3.1 g/cm^3, dimensions of the simulation cell are 16.3 Å × 16.8 Å × 16.1 Å. The box is almost rectangular, 88° < α, β, γ < 92°. Blue circles are Si, green circles are N atoms.

energy. Within the available time-scale of the ab initio molecular dynamics simulation, 20–50 ps corresponding to 20.000–50.000 time steps, we found the lowest energy configuration of all of our models at 2000 °C after 10–20 ps. Further annealing at temperatures exceeding 2400 °C results in a deterioration of the network structure, producing N–N and Si–Si bonds, and generally yielding energetically unfavorable structures. To allow further comparison and validation, we have simulated a-Si_3N_4 also by the standard melt-quench method using ab initio molecular dynamics only (*AI*-models). We will soon give a detailed account on these studies, however, deriving a suitable model without N–N or Si–Si bonds proved to be very difficult within the available simulation time (20–50 ps). We needed to apply a delicate temperature program and to monitor the disappearence of N–N bonds, before proceeding with the next temperature step. *AI*-models that fulfill our principle requirement of exhibiting no homo-atomic bonds are quite dense, above 3.0 g/cm^3. *AI*-models with low density all exhibit N–N bonds, in some cases N_2 molecules are found in internal voids. Furthermore, the amount of topological defects in *AI*-models are on average larger than in network-derived models.

The model presented in Fig. 3 comprises 448 atoms and a volume of 4.6 nm^3. Given the computational demands to treat nitrogen with its deep 2p states correctly, this model of a-Si_3N_4 comprises the current maximum size for doing ab initio molecular dynamics within the framework of density functional theory using a super computer. The model has been annealed for 10 ps at 1600 °C and the intermediate optimized structure yields the pair correlation function $g(r)$, full and pair-wise, of a-Si_3N_4 in Fig. 4. The first Si–N distance peak is located at 172 pm, but is asymmetric tailing out to longer bond distances at 210 pm and slightly beyond. Second nearest neighbor peaks are found for N–N at 273 pm, and for Si–Si at 295 pm (averaged value). There is a pronounced structure corresponding to the third nearest neighbor peak of Si–N correlations at 345 pm and 417 pm, resembling to some extend the Si–N bond distances of α- and β-Si_3N_4. A medium-range order can be observed at even further distances, up to 500 in the N–N pair distribution. We obtained similar $g(r)$ for 112-atom models from an ab initio molecular dynamics at room temperature. Within the scope of these models, $g(r)$ does not depend significantly on the density up to the limit of significant correlation distances, about 500 pm.

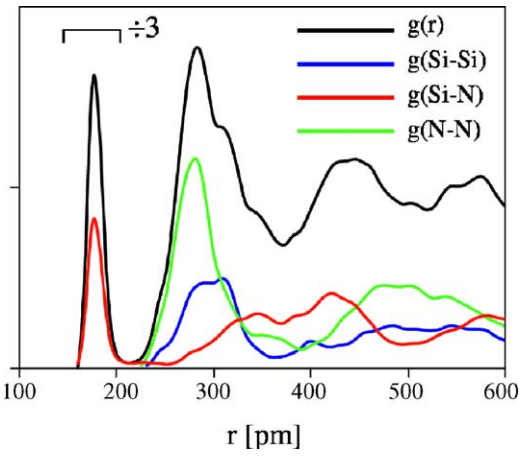

Fig. 4. Pair correlation function $g(r)$ for the 448-atom model of a-Si_3N_4.

Calculating the energy difference between the amorphous model and the crystalline reference state of β-Si_3N_4 yields the free internal energy ΔE_f. ΔE_f should neither be confused with the Helmholtz free energy ΔF (or ΔA) nor with the Gibbs free energy ΔG, the free enthalpy of a system. ΔE_f is the internal energy released upon crystallization, and besides entropy one of the major constituents to the free enthalpy, ΔG. ΔE_f is plotted as a function of density for several network-derived and *AI*-models of a-Si_3N_4 in Fig. 5 on the left. We note that the lowest energy, ΔE_f = 0.27 eV/atom or 180 kJ/mol, is achieved within both approaches to model the amorphous state of a-Si_3N_4. While such models have a density comparable to that of β-Si_3N_4, there is a trend that low-density models have a higher ΔE_f. Since we observed the formation of voids and pores in such low-density models, the increase of ΔE_f upon density decrease can be attributed to the energy necessary to create such internal surfaces.

Another quantity that depends on the density of the model is the bulk modulus, B_0. B_0 is then plotted as a function of density for models of a-Si_3N_4 in Fig. 5 on the right. For high-density models, B_0 approaches 70–75% of B_0 of β-Si_3N_4 (247 GPa). Models with lower density exhibit an – as expected – lower B_0. Interestingly, network-derived models tend to slightly larger values of B_0 in comparison to *AI*-models, probably indicating the larger amount of structural defects present in the latter ones.

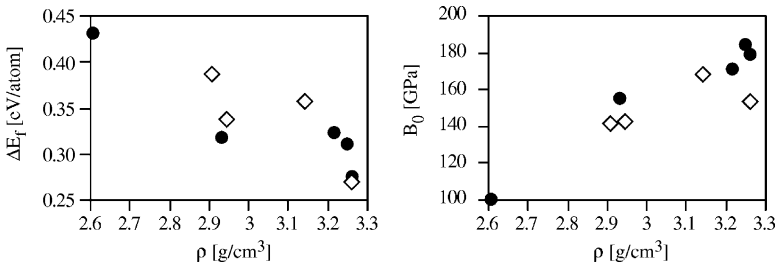

Fig. 5. Left: free internal energy ΔE_f plotted as a function of density for several models of a-Si_3N_4. Right: bulk modulus B_0 plotted as a function of density for several models of a-Si_3N_4. Filled circles correspond to models derived from networks. Open diamonds correspond to models generated via the melt-quench procedure using ab initio molecular dynamics only.

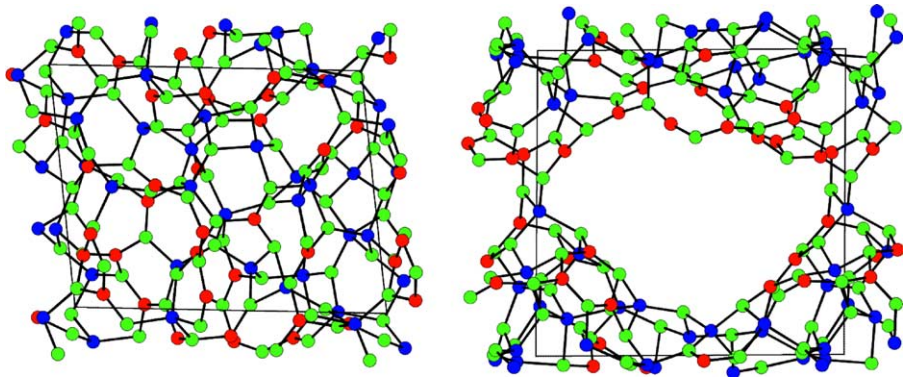

Fig. 6. Two models of a-$Si_3B_3N_7$ with 104 atoms each in the simulation cell. The model on the left side has the density $\rho = 2.8\,g/cm^3$, the one on the right has $\rho = 1.8\,g/cm^3$. Dimensions of the simulation cell are 12.5 Å × 9.3 Å × 9.1 Å, and 11.7 Å × 11.6 Å × 11.4 Å, respectively. Blue circles are Si, green circles are N, and red circles are B atoms, respectively.

3.2. *a-$Si_3B_3N_7$*

Two representative models of a-$Si_3B_3N_7$ are shown in Fig. 6. Very similar to our experience in the course of modelling a-Si_3N_4 we obtain a pore within models of very low densities. Low-density structures of a-$Si_3B_3N_7$, however, are significantly easier to construct than for a-Si_3N_4 due to the lower average network connectivity of $Si_3B_3N_7$. With 104 atoms in the simulation cell, we could generate models with densities ranging from $\rho = 2.8\,g/cm^3$ to $\rho = 1.8\,g/cm^3$ as perfect inorganic networks. Experimental values for ρ are reported within the range of 1.8–2.1 g/cm^3.[4]

As a similar trend found for a-Si_3N_4, the networks of a-$Si_3B_3N_7$ also gained energy during the optimization and annealing procedure. The overall gain, however, was less. Furthermore, we find significantly less topological defects in a-$Si_3B_3N_7$. Although our data is not as good supported by larger scale models as for a-Si_3N_4, we find about 8% for defects such as $N^{[4]}$ and $B^{[4]}$, and about 4% for defects such as $N^{[2]}$, $B^{[2]}$, and $Si^{[5]}$. We usually find no $Si^{[3]}$ and observe a much smaller variation of Si–N bond distances than in a-Si_3N_4. There is some trend for increasing defect concentration with decreasing density of the model.

Fig. 7 shows the pair correlation function for a-$Si_3B_3N_7$ as received in a ab initio molecular dynamics at room temperature. Table 1 lists the maxima of the individual atom–atom distance distributions that can be derived by inspecting the individual contributions to $g(r)$. The results correspond very well with the analysis of neutron scattering data given by Hagenmayer et al.[21] It is worthy to note that in the modelling we are able to trace the Si–(N)–B distance (285 pm) of the second coordination shell that interferes with the N–(Si)–N peak at 276 pm. Our value, however, is somewhat larger than the 274 pm used by van Wüllen et al. for the fitting and interpretation of their NMR data.[22]

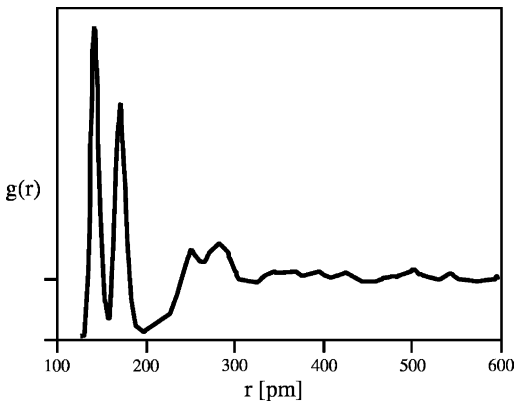

Fig. 7. Pair correlation function $g(r)$ of a-$Si_3B_3N_7$ calculated from an ab initio molecular dynamics at room temperature.

Table 1
Maxima of atom–atom correlations in a-Si_3 B_3N_7

Atom–atom correlation	Distance of maximum (pm)
B—N	144
Si—N	173
B—*N*—B	250
N—*B*—N	252
N—*Si*—N	276
B—*N*—Si	285
Si—*N*—Si	292
N—*B*—*N*—B	320
Si—*N*—*B*—N	350
N—*Si*—*N*—B	370
Si—*N*—*Si*—N	410

Bridging atoms are in italics.

Table 2
Second neighbor coordination numbers in a-Si_3 B_3N_7

Atom–atom correlation	Random statistics	Simulation	Experiment
Si—*N*—Si	4.6	5.1	6.5 ± 0.5
B—*N*—B	2.6	2.8	4.5 ± 0.5
Si—*N*—B	3.4	2.8	1.3 ± 0.2

The values for the random statistics are computed assuming Si four-fold coordinated by N and B three-fold coordinated by N, while N is three-fold coordinated by Si and B. The numbers for the simulated model do not sum up to exactly 8 or 6 for Si and B, respectively, because of four-membered rings present in the model.

Nevertheless, the genuine trend of structural partitioning in a-Si_3 B_3N_7 established by van Wüllen et al. from an extensive NMR study[22] is found in our models as well. To illustrate this, we show a porous model of a-$Si_3B_3N_7$ emphasizing the BN-substructure in Fig. 8. All B atoms in this model have agglomerated in just two large BN fragments, one of which can be thought of being condensed of borazine rings. And indeed, although constructed as random networks, the structures that we obtained after extensive ab initio molecular dynamics at elevated temperatures (20–40 ps at 2000 °C) are no random networks anymore. On the contrary, we observe significant deviation from random statistics in the second nearest neighbor coordination of Si–(N)–Si, Si–(N)–B, and B–(N)–B. Our computational results are given in Table 2 together with those received in the experiment.

Fortunately, the models yield some further information about the BN-segregations in a-$Si_3B_3N_7$. As visible in Fig. 8, the BN-rich segregations in all porous models are predominantly found at the internal surfaces of a pore. Complementary, there is a significant depletion of B atoms within the bulk-framework of the structure as illustrated in Fig. 9. We found two reasons for this tendency to phase separate. For one the systems attempts to gain a maximum in bonding energy. Thus, increasing the π-overlap of co-planar B–N bonds favors extended BN regions that resemble structural fragments of h-BN. The observation that all BN-segregations are located at the internal surfaces, however, points out a second driving force. A low-density model of a-$Si_3B_3N_7$ unavoidably contains voids and pores. Such parts of the microstructure result in surface structures, locally two-dimensional. A surface, however, is always associated with a typical energy needed to create this interface. The h-BN-like structural fragments are then the only constituents of the structure that can minimize the local stresses that such a surface imposes.

This effect becomes, furthermore, visible when plotting the free internal energy ΔE_f of the amorphous phase as a function of the density ρ, see Fig. 10. ΔE_f is given with reference to the crystal phases β-Si_3N_4 and h-BN. At first glance, the dependence of ΔE_f of ρ is similar to that already seen for a-Si_3N_4 in Fig. 5: ΔE_f increases with decreasing density ρ. A quantitative comparison, however, shows that it takes less energy to blow up $Si_3B_3N_7$ than a-Si_3N_4. Furthermore, the steady increase of ΔE_f appears to stop at $\rho \approx 2.2$ g/cm^3, that is with the appearance of larger pores. Once such a large pore is formed, the structure eventually comprises a porous SiN-rich framework structure with its surfaces coated by BN-rich segregations. Further decreasing the density has no or signif-

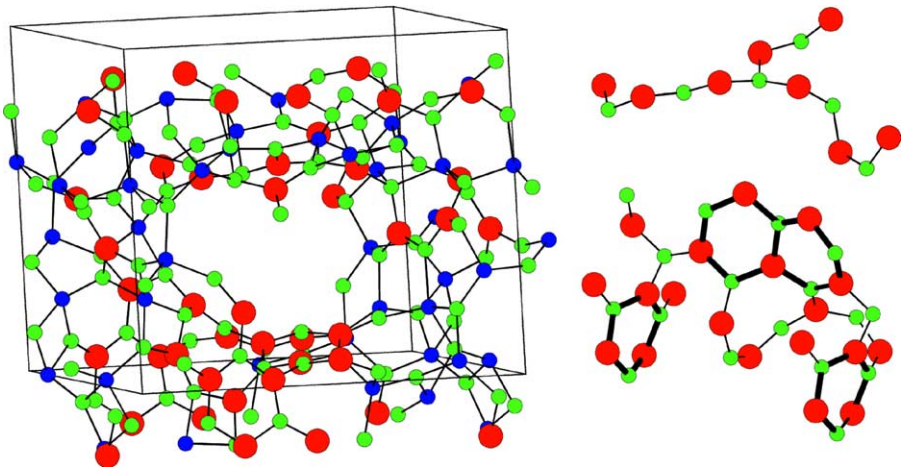

Fig. 8. A porous model of a-$Si_3B_3N_7$. The full structure is shown on the left, two structural fragments consisting of B and N only are repeated on the right. Si, N, and B are blue, green, and red circles, respectively.

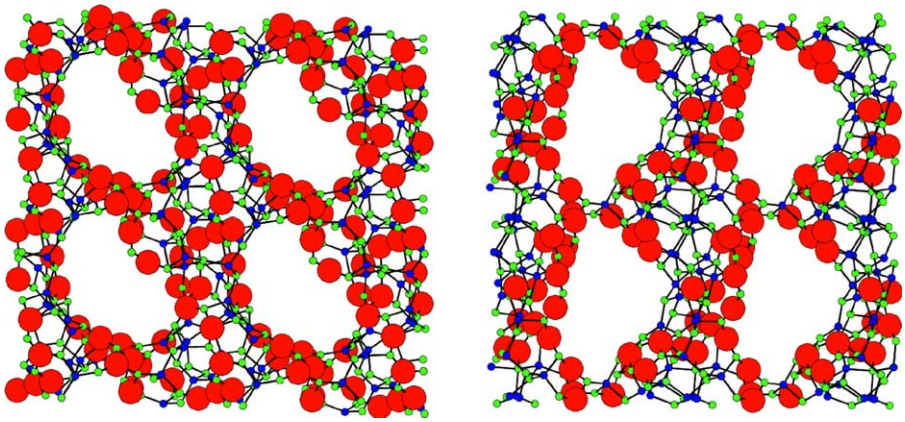

Fig. 9. Two different porous models of a-$Si_3B_3N_7$ (each a 2 × 2 × 1 supercell) illustrating preferential BN-segregation at internal surfaces of the structure, and BN-depletion of the bulk framework. B atoms are represented by large red balls, while Si and N atoms are small blue and green circles, respectively.

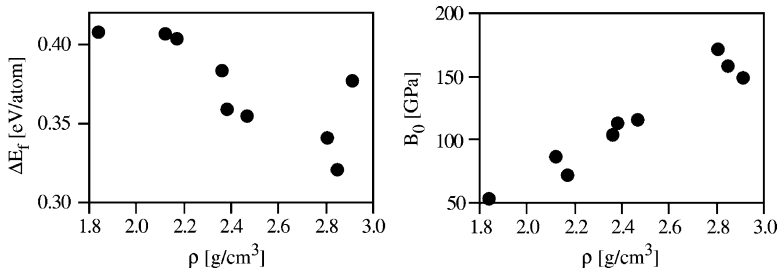

Fig. 10. Left: free internal energy ΔE_f plotted as a function of density for several models of a-$Si_3B_3N_7$. The crystal reference is taken as β-Si_3N_4 and 3 h-BN. Right: bulk modulus B_0 plotted as a function of density for several models of a-$Si_3B_3N_7$.

icantly less impact on the energy of the structure, unless the model is not ruptured completely.

The bulk modulus B_0 of the a-$Si_3B_3N_7$ models is then plotted in Fig. 10 on the right side. We observe the obvious trend of increasing B_0 with increasing density ρ. The largest value of B_0 we calculated, 173 GPa, almost matches B_0 of a-Si_3N_4 at 8% less density. Taking a different perspective, at a given density ρ, B_0 of a-$Si_3B_3N_7$ comes out about 20% larger than B_0 of a-Si_3N_4.

3.3. *a-SiNO*

To study the Si–N–O phase system we scanned the complete range of compositions from SiO_2 to Si_3N_4 modelling each three to five structures for 17 intermediate compositions. Two structural models of a-SiNO with very different compositions are shown in Fig. 11. In previous publications we noted that we retain the perfect network structure without defects up to a composition of $Si_{49}N_{52}O_{20}$ even after extended ab initio

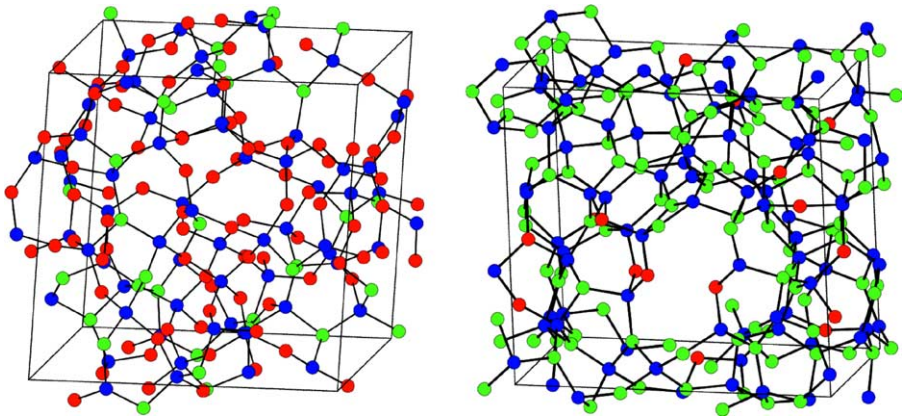

Fig. 11. Two models of a-SiNO. The model of the left side has the composition $Si_{40}N_{16}O_{56}$, a density of 2.3 g/cm^3, and cell dimensions 11.8 Å × 11.8 Å × 11.6 Å. The model on the right side has the composition $Si_{51}N_{60}$ O_{12}, a density of 2.8 g/cm^3, and cell dimensions 11.4 Å × 12.1 Å × 10.6 Å. The boxes are close to rectangular, 86° < α, β, γ < 93°. Si, N, and O are blue, green, and red circles, respectively.

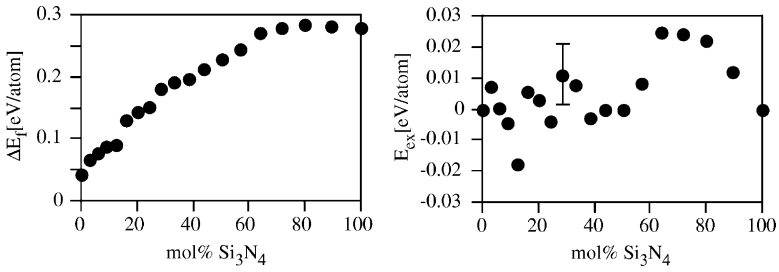

Fig. 12. Left: free internal energy, ΔE_f, of a-SiNO plotted as a function of mol% Si_3N_4. Right: the excess energy, E_{ex}, of the a-SiNO phase if decomposed into appropriate amounts of amorphous SiO_2, Si_2N_2O, and Si_3N_4. The error bar indicates the estimated uncertainty of a single point.

molecular dynamics simulations at 2000 °C. Therefore, the a-SiNO networks we produce with the empirical generation scheme do relax to some extend during the optimizing and annealing procedure, but they do not change their topology. The energy released during the optimization corresponds to not more than an intrinsic thermal energy of 1000 °C. Structures with a higher content of nitrogen, thus approaching the boundary of Si_3N_4, show an increasing tendency for network rearrangements indicated by formation of new bonds as well as bond breaking. The net result is that some atoms become over-coordinated ($Si^{[5]}$, $N^{[4]}$, $O^{[3]}$) and some two-coordinated N atoms appear. The three-coordinated Si appeared in none of the models containing oxygen. We are currently in the progress of modelling a-SiNO for some intermediate compositions using the standard *melt-quench* approach and ab initio molecular dynamics only. The structures we received so far have more defects and are less favorable in energy than corresponding network models. For more details on the structure of a-SiNO we refer to a recent report.[23]

The current state of our investigation of the free internal energy, ΔE_f, of a-SiNO is shown in Fig. 12. ΔE_f is defined as the energy difference between a crystalline reference state composed of appropriate amounts of quartz-SiO_2, Si_2N_2O, and β-Si_3N_4 and the amorphous phase. The reference energies for quartz-SiO_2 Si_2N_2O, and β-Si_3N_4 are computed to −26.15 eV, −45.02 eV, and −63.57 eV per formula unit, respectively. Note that we incorporated only one data point for each composition, that with lowest energy we found. The density along the data points is interpolated approximately linearly between 2.2 g/cm^3 for a-SiO_2 and 3.2 g/cm^3 for a-Si_3N_4. For a-SiO_2 the calculated value of 0.04 eV/atom is comparable to experimental data obtained from calorimetric measurements.[24] For pure a-Si_2N_2O or a-Si_3N_4 no such value has been measured. Our values of about 0.23 eV/atom and 0.27 eV/atom for the free internal energy of a-Si_2N_2O and a-Si_3N_4, respectively, reflect the different chemistry and the higher connectivity of the network structure of the nitrogen-rich compounds in comparison to a-SiO_2.

The data provided in Fig. 12 carries even more information. To zeroth order the diagram suggests a linear relation of ΔE_f for compositions intermediate between SiO_2 and Si_2N_2O, while there is a different relation between Si_2N_2O and Si_3N_4. The first trend is expected from an ideal mixture of SiO_2 and Si_2N_2O according to Vegard's rule. A deviation from linearity becomes more pronounced, if we calculate a quantity that we call excess (internal) energy E_{ex} of the a-SiNO phase. E_{ex} is calculated the same way as ΔE_f, however, instead of the energies of the crystal phases we use the energies of the amorphous phases of SiO_2 Si_2N_2O, and Si_3N_4 (−26.03 eV, −43.87 eV, and −61.67 eV per formula unit, respectively; see the reported values above). Hence, E_{ex} becomes zero for these three compositions. E_{ex} may then be interpreted as an energy measure that indicates how easily two amorphous phases will mix with each other. The free enthalpy ΔG of the system then includes also entropy contributions of various sources. This resulting diagram is shown in Fig. 12 on the right side. We first note that E_{ex} is a small quantity in comparison to ΔE_f The actual value of E_{ex}, furthermore, is affected by systematic errors of theory and modelling procedure as well as by statistical errors of the data. Nevertheless, within the estimated generous error, say 0.01 to 0.02 eV/atom, the graph of Fig. 12 supports a miscibility of the amorphous phases of SiO_2 and Si_2N_2O. On the other hand, it corroborates the idea of a pronounced miscibility gap between Si_2N_2O and Si_3N_4, especially by judging the smooth appearance of the data points. Interestingly, there is a data point at 12.5 mol% Si_3N_4 corresponding to 25 wt.% Si_3N_4 that singles out in the a-SiNO diagram. While it is well included within the estimated error, it may nevertheless lead to some speculation that we will discuss.

The bulk modulus B_0 of a-SiNO is plotted in Fig. 13. We have recently given a detailed account of the compress-

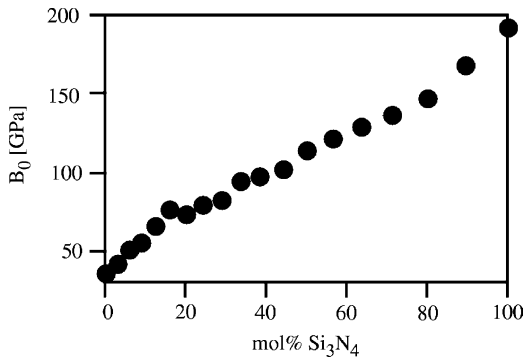

Fig. 13. Bulk modulus B_0 of a-SiNO plotted as a function of mol% Si_3N_4.

ibility in a-SiNO, pointing out a coincidence of Si–N bond percolation and network softening.[25] This effect happens for about 16 mol% or 31 wt.% Si_3N_4 in a-SiNO and is visible in Fig. 13 as well. When starting with a-SiO_2 there is an almost linear increase of B_0 with increasing Si_3N_4-content until the Si–N bond percolation occurs. Beyond this point, at which B_0 suddenly decreases, there is a second regime of linear relation with a slower increase up to about 80 mol% Si_3N_4. Approaching the phase boundary of Si_3N_4 gives rise to a steeper increase of B_0 again.

3.4. a-SiCN

In the previous sections we studied compounds that correspond to inorganic networks perfectly alternating in cations and anions. This posed a challenge to the modelling procedure, because a perfect alternation requires a network with even-membered rings only. Odd-membered rings, hence, must be excluded at any times to omit homo-atomic bonds. The chemistry of such compounds is rather simple in such a way, that only a few kinds of different bonds exist. Only Si–N bonds are present in a-Si_3N_4, $Si_3B_3N_7$ or a-SiNO comprise two kinds of bonds, Si–N and B–N bonds or Si–N and Si–O, respectively. The ternary Si–C–N system, on the other side, comprises a much wider variety of bonds. Suppressing the homo-atomic Si–Si and N–N bonds – to reflect that we stay behind the tieline Si_3N_4–SiC in the phase diagram – we generated network models with Si–N, Si–C, C–N, and C–C bonds. An additional parameter that needs to be addressed are the proportions of so-called sp^3 and sp^2 carbon atoms. Although the variety appears to be limited at a first glance, it nevertheless leads to a combinatorial explosion of different bonding configurations possible in a model.

Our approach to model a-SiCN then addressed the hybridization of carbon and the question, how sensitive the optimized models that we obtain after the optimization and annealing procedure are to the initial condition provided by the empirically generated network model. We ran two sets of four simulation models each. Each model within one set is distinguished by different proportions of so-called sp^3 and sp^2 carbon, pre-configured by the empirical network. The two sets differ by the density provided. We choose the composition of a-$Si_{40}C_{40}N_{40}$, the center of the ternary phase diagram. Fig. 14 then shows two of the resulting eight structures of a-$Si_{40}C_{40}N_{40}$.

At this point we can only summarize the basic trends we observed for our models, a more detailed account of structures and their evolution during the ab initio molecular dynamics at elevated temperatures will be given elsewhere. As a first result we found that the proportions of sp^3 and sp^2 carbon soon converged within the four models with similar density. Thus, although pre-configured as random networks by the empirical generation scheme with proportions of 36:4, 24:16, 12:28, and 0:40 for the ratio sp^3-C:sp^2-C, the optimization and annealing procedure balanced out the hybridization. Nevertheless, two parameters determine the ratio sp^3-C:sp^2-C. First, it is a function of temperature used in the ab initio molecular dynamics simulation. After annealing at 800 °C we found about 75% of all C as sp^3-C, while after 40 ps ab initio molecular dynamics at 2000 °C this proportion was decreased to merely 40%. These values, however, are for the high-density models of a-$Si_{40}C_{40}N_{40}$ with $\rho = 2.8$ g/cm^3 only. The low-density models, ρ = 2.2–2.5 g/cm^3, exhibit significantly smaller amounts of sp^3-C. Just 50% after annealing at 800 °C and 25% after 40 ps ab initio molecular dynamics at 2000 °C. Therefore, the second trend we observe is the dependence of the proportions of sp^3 and sp^2 on the density of the model.

The change of the ratio sp^3-C:sp^2-C goes along with substantial reorganizations of the network. During the course of annealing we observe C–N bond breaking and C–C bond formation. C atoms agglomerate locally and SiN-rich regions

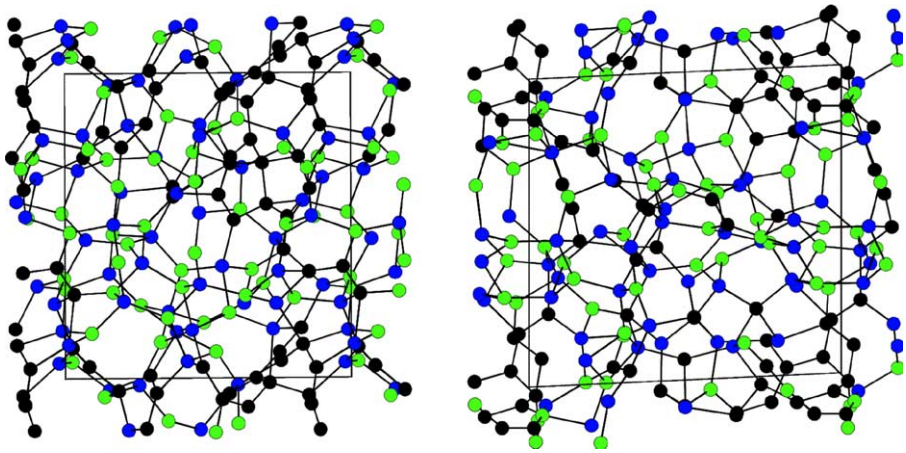

Fig. 14. Two models of a-$Si_{40}C_{40}N_{40}$. The model of the left side has a density of 2.9 g/cm^3, and cell dimensions 11.2 Å × 10.5 Å × 10.2 Å. The model on the right side has a density of 2.5 g/cm^3, and cell dimensions 11.4 Å × 11.0 Å × 11.5 Å. The boxes are close to rectangular, 85° < α, β, γ < 92°. Blue, green, and black circles represent Si, N, and C atoms, respectively.

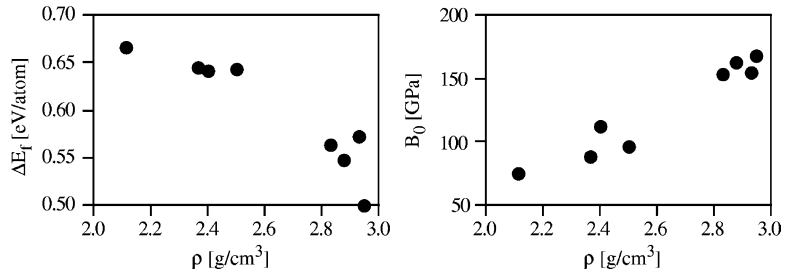

Fig. 15. Left: free internal energy, ΔE_f, plotted as a function of density for several models of a-SiCN with composition a-$Si_{40}C_{40}N_{40}$. The crystal reference is taken as β-Si_3N_4, β-SiC, and g-C. Right: bulk modulus B_0 plotted as a function of density for several models of a-SiCN with composition a-$Si_{40}C_{40}N_{40}$.

become visible, even in the models shown in Fig. 14. There appears to be a trend for C-segregation at internal surfaces of voids and pores in low-density structures, but less obvious as for a-$Si_3B_3N_7$ due to remaining C atoms in the bulk framework. This partitioning of the network, to some extend similar to that already observed for a-$Si_3B_3N_7$, goes along with a steady decrease of the internal energy. We plot the free internal energy ΔE_f of models obtained after 40 ps ab initio molecular dynamics at 2000 °C as a function of density for models of a-$Si_{40}C_{40}N_{40}$ in Fig. 15, on the left side. As noted in previous section, we observe the distinct trend of increasing ΔE_f with decreasing density.

Most noteworthy, however, is the very different value of ΔE_f. With crystal phases of β-Si_3N_4, β-SiC, and g-C taken as reference, the lowest value of ΔE_f is about 0.5 eV/atom. This is about twice the value we obtained for a-Si_3N_4 or a-$Si_3B_3N_7$. We can compare ΔE_f of a-$Si_{40}C_{40}N_{40}$ with ΔE_f for some boundary phase in the phase diagram, that we obtained in a very similar way: a-SiC (0.21 eV/atom), a-C (0.17 eV/atom), a-(Si_3N_4 + 3SiC) (0.40 eV/atom), and a-Si_3N_4:C (0.29 eV/atom).[26] Obviously, our models of a-$Si_{40}C_{40}N_{40}$ are quite unfavorable in energy, although annealed and optimized. Further annealing at temperatures exceeding 2400 °C resulted in deteriorated networks with higher energy. We can draw a conclusion if we look at the nature of our model of a-Si_3N_4:C presented in a previous publication.[26] We inserted a graphitic strip of carbon into a matrix consisting of a-Si_3N_4 and found that ΔE_f (per atom) did not increase significantly. Therefore, the results we obtain for a-SiCN support the conclusion that the solubility of carbon in a-Si_3N_4 or a-SiCN is suppressed. Values of ΔE_f suggest a high driving force for a partitioning of the a-SiCN network towards a stoichiometric a-SiCN and graphitic-C. This driving force is significantly higher than for $Si_3B_3N_7$ or Si_2N_2O.

The bulk modulus B_0 of the a-$Si_{40}C_{40}N_{40}$ models is then plotted in Fig. 15 on the right side. The increase of B_0 with increasing density ρ is, once more, obvious. The largest value of B_0 we calculated, 168 GPa, approaches B_0 of a-Si_3N_4, but for a structure with 7% less density. Taking the different perspective: B_0 of a-$Si_{40}C_{40}N_{40}$ comes out similar to B_0 of a-$Si_3B_3N_7$ or about 20% larger than B_0 of a-Si_3N_4 for a given density ρ.

4. Discussion

The combination of empirical and quantum mechanical methods allows to study the amorphous structure of polymer-derived ceramics in an efficient and accurate way. Models generated by standard melt-quench methods using ab initio molecular dynamics simulations only have a higher concentration of structural defects and, most awkward in nitrogen containing materials, very often exhibit N–N bonds. The network approach is not only appealing by its concept – in syntheses molecules and polymers form inorganic networks by cross-linking – but also by its speed and its capabilities: a complete phase diagram may be derived and validated as we did for a-SiNO or a manifold of different hypotheses may be tested as seen for structures of a-SiCN. The latter technique can further be used for questions concerning the persistence of local fragments in the amorphous state. It is worthy to note in this context that the employment of quantum mechanical methods proved to be mandatory for atomistic simulations of disordered covalent materials. While the structure of silica glass can be modelled using simple and fast potential approaches, an empirical method certainly will fail in the treatment of structural defects (under- and over-coordination of atoms) and dynamical evolution (bond rupture and formation as well as corresponding transition states). The latter point is one to worry about when using empirical potentials. All structural models of silicon nitride ceramics derived and published so far exhibit an extra-ordinary high proportion of under-coordinated silicon. Though this is balanced out by over-coordination to yield the “correct” average connectivity, it is nevertheless a severe imperfection. Furthermore, such models can not be used for further chemical studies, e.g. assessment of reactivity in the solid state or catalysis.

It is interesting that the random network structure, which is the underlying idea of the modelling scheme, is not supported by the final results both for a-$Si_3B_3N_7$ and a-SiCN. In both compounds, we could detect the trend to partition quite clearly and show that it is energetically driven. The driving force for a-SiCN materials to phase separate then appears to be much larger than for a-$Si_3B_3N_7$. Given the values of the excess energy with reference to the constituting phases in their amorphous state as well as our results of a model of carbon segregation in a-Si_3N_4, we conclude that carbon is

not solvable in stoichiometric a-SiCN. Consequently, seeds of graphitic segregation will develop in a very early state. Our data, however, currently does not allow for an assessment of the kinetics of such systems. The results, however, encouraged us to further improve our modelling scheme and to implement techniques to bias the network evolution during the empirical generation.

The calculated free internal energy of our amorphous models may be taken as a measure for the enthalpy such compounds loose during crystallization. This certainly holds for a-SiO_2, which is a glass and can be synthesized with high purity. Since any kind of impurity element will decrease the energy of the amorphous structure, our results, however, have to be taken with some care. The most predominant element found in polymer-derived materials is, of course, hydrogen. Our studies on hydrogenated silicon nitride have already shown that hydrogen decreases the free internal energy significantly.[11] This holds for a-SiCN as well: 25 at.% H corresponding to just 3 wt.% decrease the free internal energy by about 50%. Thus, hydrogen will play a significant role for the stability, both kinetic and thermodynamical, of the compound. It should not be forgotten that contributions of entropy from various sources (mixing, structural, vibrational, electronical) further add to the free enthalpy ΔG of the system.

Such entropy terms will certainly dominate glassy stoichiometric a-SiNO-phases. A rough estimate of mixing entropy yields a contribution of 0.1 eV/atom for a-Si_2N_2O at a temperature of 1000 K. Thus, the data we provided in Fig. 12 on left side, may be taken to determine the solubility of Si_3N_4 in silica glass. The existence of a-Si_2N_2O itself appears unlikely given that ΔE_f is larger than 0.2 eV/atom. If it would exist, we would expect full miscibility of a-SiO_2 and a-Si_2N_2O as indicated in Fig. 12 on the right side. The data for 12.5 mol% Si_3N_4 in this diagram, furthermore, indicates a local region of stability—if it were not for the uncertainty of the modelling procedure. Interestingly, this corresponds to the composition of an a-SiNO-glass reported by Kohn et al.,[27] although Gu et al.[28] argued against such a far extension of solubility. Nevertheless, the data point motivates us to study this region further and, moreover, search for possible crystalline remnants with this composition of $Si_5N_2O_7$.

The results we obtain for the bulk modulus of the compounds follow the expectation and experimental experience. For one, elasticity scales with the density of the material. Secondly, one of the advantages of a-$Si_3B_3N_7$ and a-SiCN materials is that they exhibit similar mechanical properties as a-Si_3N_4 but at lower density of the material. The bulk modulus, however, is only a rough measure for the hardness of a material and there is still a necessity to investigate the behavior of the amorphous phase under shear as well as its adhesion to a supporting material.

The capabilities of computational resources together with the network generation scheme point towards simulations of phenomena at the length scale of nanometers. The very large model of a-Si_3N_4 with 448 atoms has a volume of almost 5 nm^3 and can be utilized to investigate the effect of small metal clusters in an amorphous matrix. Another direction is the investigation of interfaces, e.g. the thin grain boundary films in sintered silicon nitride ceramics or the metal ceramic interface in thin film coatings. Current projects we pursue go into this direction: investigation of concentration profiles along grain boundary films that may contain metals and the chemistry of the a-SiCN/α-Fe interface with trends of interfacial energy and adhesion in dependence of composition of the amorphous phase.

5. Summary

We studied structure, energy, and the bulk modulus of amorphous silicon nitride, a-Si_3N_4, and its ternary derivatives a-$Si_3B_3N_7$, a-SiNO, and a-SiCN. Model structures consisting of 104–448 atoms were derived from random networks using an empirical generation scheme and further optimized within density functional theory including extensive ab initio molecular dynamics simulations. The combination of empirical and quantum mechanical methods allowed an efficient study with highly accurate methods. As an outcome we obtain structures with perfect chemical order that comprise local environment of atoms consistent with the perception of an inorganic network. While the defect concentration in fully optimized structures is low in general, the three-coordinated silicon atom is a rare species with an abundance of about 1% and below.

After annealing at 2000 °C we find that structures of a-$Si_3B_3N_7$ and a-SiCN exhibit phase segregation of BN and C, respectively. This partitioning of the random network is driven by energy, with a significantly higher driving force for the carbon containing material. We thus conclude that carbon is not solvable in stoichiometric a-SiCN. There is, furthermore, a connection between density and segregation: low-density models of both a-$Si_3B_3N_7$ and a-SiCN exhibit voids and pores with the internal surface coated with the precipitating phase and the framework predominantly composed of a-Si_3N_4. Structural models of a-SiNO, on the other side, show no phase partitioning and the structure is consistent with a random network composed of Si–N and Si–O bonds. The dependence of energy with composition, however, indicates a miscibility gap between a-SiO_2 and a-Si_3N_4. We observe a remarkable trend for a-SiNO phases: the onset of Si–N bond percolation throughout the structure and is accompanied by a discontinuous behavior of the bulk modulus and an intermediate softening of the structure.

The results of this study show that the approach of network-derived models provide perspectives towards more complex problems: defects and phase separation in amorphous materials, metal–ceramic interfaces, and clusters embedded in the amorphous phase are prospects that can now be tackled and that merit investigation.

Acknowledgments

The author is indebted to many people, especially Ralf Riedel, Rishi Raj, and Richard Dronskowski for their continuous support and encouragement to pursue this work. Financial support came from the Fonds der Chemischen Industrie (FCI) and the Deutsche Forschungsgemeinschaft (Kr1805/3-1 and 4-2). The computational work was only made possible by very generous grants by the FZ Jülich and the Computer and Communication Center at Aachen.

References

1. Bill, J. and Aldinger, F., *Adv. Mater.*, 1995, **7**, 775.
2. Riedel, R., *Materials Science and Technology*, *Vol 17B*, ed. R. W. Cahn, P. Haasen and E. J. Kramer. VCH Weinheim, 1996, pp. 2–50.
3. Riedel, R., Kleebe, H.-J., Schönfelder, H. and Aldinger, F., *Nature*, 1995, **374**, 526.
4. Baldus, H. and Jansen, M., *Angew. Chem. Int. Ed. Engl.*, 1997, **36**, 328.
5. Zachariasen, W. H., *J. Am. Chem. Soc.*, 1932, **54**, 3841.
6. Umesaki, N., Hirosaki, N. and Hirao, K., *J. Non-Cryst. Solids*, 1992, **150**, 120.
7. de Brito-Mota, F., Justo, J. F. and Fazzio, A., *Phys. Rev. B*, 1998, **58**, 8323.
8. Matsunaga, K., Iwamoto, Y., Fisher, C. A. J. and Matsubara, H., *J. Ceram. Soc. Jpn.*, 1999, **107**, 1025.
9. Amkreutz, M. and Frauenheim, T., *Phys. Rev. B*, 2002, **65**, 134113.
10. Sarntheim, J., Pasquarello, A. and Car, R., *Phys. Rev. Lett.*, 1995, **74**, 4682.
11. Kroll, P., *J. Non-Cryst. Solids*, 2001, **293–295**, 238.
12. Hohenberg, P. and Kohn, W., *Phys. Rev. B*, 1964, **136**, 864.
13. Payne, M. C., Teter, M. P., Allan, D. C., Arias, T. A. and Joannopoulos, J. D., *Rev. Mod. Phys.*, 1992, **64**, 1045.
14. Kresse, G. and Hafner, J., *Phys. Rev. B*, 1993, **47**, 558.
15. Kresse, G. and Hafner, J., *Phys. Rev. B*, 1994, **49**, 14251.
16. Kresse, G. and Furthmüller, J., *Comput. Mater. Sci.*, 1996, **6**, 15.
17. Kresse, G. and Furthmüller, J., *Phys. Rev. B*, 1996, **54**, 11169.
18. Kroll, P., *J. Mater. Chem.*, 2003, **13**, 1657.
19. Kroll, P., *Mater. Res. Symp. Proc.*, 2002, **731**, 255.
20. Searle, T., ed., *Properties of Amorphous Silicon and its Alloys*. INSPEC, London, 1998 [and references therein].
21. Hagenmayer, R. M., Müller, U., Benmore, C. J., Neuefeind, J. and Jansen, M., *J. Mater. Chem.*, 1999, **9**, 2865.
22. van Wüllen, L., Müller, U. and Jansen, M., *Angew. Chem. Int. Ed.*, 2000, **39**, 2519.
23. Kroll, P., *J. Non-Cryst. Solids*, in press.
24. Mao, H., Sundman, B., Wang, Z. and Saxena, S. K., *J. Alloys Comp.*, 2001, **327**, 253.
25. Kroll, P., *J. Non-Cryst. Solids*, accepted for publication.
26. Kroll, P., *Mater. Res. Symp. Proc.*, 2002, **731**, 249.
27. Kohn, S., Hoffbauer, W., Jansen, M., Franke, R. and Bender, S., *J. Non-Cryst. Solids*, 1998, **224**, 232.
28. Gu, H., Cannon, R. M., Seifert, H. J., Hoffmann, M. J. and Tanaka, I., *J. Am. Ceram. Soc.*, 2002, **85**, 25.